Optimizing Multiplexed Detections of Diabetes Antibodies via Quantitative Microfluidic Droplet Array

Kai Duan, Gargi Ghosh, and Joe Fujiou Lo*

Sensitive, single volume detections of multiple diabetes antibodies can provide immunoprofiling and early screening of at-risk patients. To advance the state-of-the-art suspension assays for diabetes antibodies, porous hydrogel droplets are leveraged in microfluidic serpentine arrays to enhance reagent transport. This spatially multiplexed assay is applied to the detection of antibodies against insulin, glutamic acid decarboxylase, and insulinoma-associated protein 2. Optimization of assay protocol results in a shortened assay time of 2 h, with better than 20 pg mL Supporting Information detection limits across all three antibodies. Specificity and cross-reactivity tests show negligible background, nonspecific antibody–antigen, and nonspecific antibody–antibody bindings. Multiplexed detections are able to measure within 15% of target concentrations from low to high ranges. The technique enables quantifications of as little as 8000 molecules in each 500 µm droplet in a single volume, multiplexed assay format, a breakthrough necessary for the adoption of diabetes panels for clinical screening and monitoring in the future.

1. Introduction

The role and function of the rising levels of autoantibodies in Type I diabetes (T1D) is of great interest to the disease pathogenesis. Detection of diabetes autoantibodies enables clinical diagnosis of T1D,[1–10] and sensitive detections have the potential to provide predictive and screening values.[10–13] Autoantibodies against insulin, glutamic acid decarboxylase (GAD), and insulinoma associated protein-2 (IA-2) are well established in T1D panels, and thus are targeted in multiplexed detections.[14,15] The presence of IA-2 antibodies in clinical T1D ranges from 54% to 75%.[16] Additionally, 66% of newly diagnosed patients test positive for insulin autoantibody.[17] Testing for a panel of aforementioned antibodies using sensitive detections can identify better than 85% of disease presentation or future T1D development with 98% specificity.[18] Moreover, T1D accounts for more than 80% of diabetes in young children.[19]

K. Duan, Prof. G. Ghosh, Prof. J. F. Lo
Bioengineering Program
Department of Mechanical Engineering
University of Michigan at Dearborn
Dearborn, MI 48128, USA
E-mail: jfjlo@umich.edu

The ORCID identification number(s) for the author(s) of this article can be found under https://doi.org/10.1002/smll.201702323.

Unsettlingly, development of T1D in children is especially acute, with afflicted children showing severe symptoms, very high blood glucose, marked glycosuria, and ketonuria.[20,21] Incidentally, the rise of autoantibodies manifests very early, with transients observable before 1 year of age (**Figure 1**A), providing a strong marker for clinical diagnosis and screening for T1D.[22] For these young patients, earlier diagnosis or even predictive screening may mean critical disease management before manifestation of life-threatening symptoms. Current understanding of these diabetes autoantibodies points to a potential neoantigen immunogenicity,[23–26] where stress-modified protein synthesis leads to new epitopes on autoantigens that enhance their bindings to antibodies[27–31] or elicit cell-mediated immune responses.[32–36] Thus, sensitive detection of insulin, GAD, and IA-2 autoantibodies can serve as a powerful diabetes panel to monitor T1D disease progression, as well as investigate the mechanisms of beta cell autoimmune dysfunctions.

The standard detection methods for diabetes autoantibodies include radioimmunoassays (RIAs) and enzyme-link immunosorbent assays (ELISAs). Serum RIA and ELISA protocols uses semi-quantitative titrations with varying sensitivities, which may not be useful for early or new-onset diabetics.[37] In practice, RIA is time consuming and labor intensive, while ELISA requires multiple sample preparations to provide multiplexed detection of autoantibodies.[1,5] Moreover, there is a need for a uniform method of quantitative detections of all three antibodies in a single volume. For example, serum autoantibody levels can be measured in dilution titers (e.g., Juvenile Diabetes Foundation units), RIA percentage, or in enzymatic U mL^{-1}, with various cutoff definitions for positive detections.[1,5,15,38] As a comparison, normal serum levels of all three autoantibodies are nominally regarded as 0.02×10^{-9} M (e.g., 2.4 ng mL^{-1} for insulin IgG) or lower by the World Health Organization and Mayo Clinic Interpretive Handbook.[39] Nevertheless, the cutoffs established by the various methods represent the diagnostic levels of T1D, whereas early screening would call for greater sensitivity to detect earlier transients.

Toward improving diabetes autoantibody detections, advances have been made via multiplexed microarrays[15] and electrochemiluminescence (ECL) assays.[14,40,41] Diabetes microarrays enabled single serum preparation for a multiplexed antibody detection panel, while ECL assays pushed the quantitative

**ADVANCED
SCIENCE NEWS**

www.advancedsciencenews.com

NANO · MICRO

small

www.small-journal.com
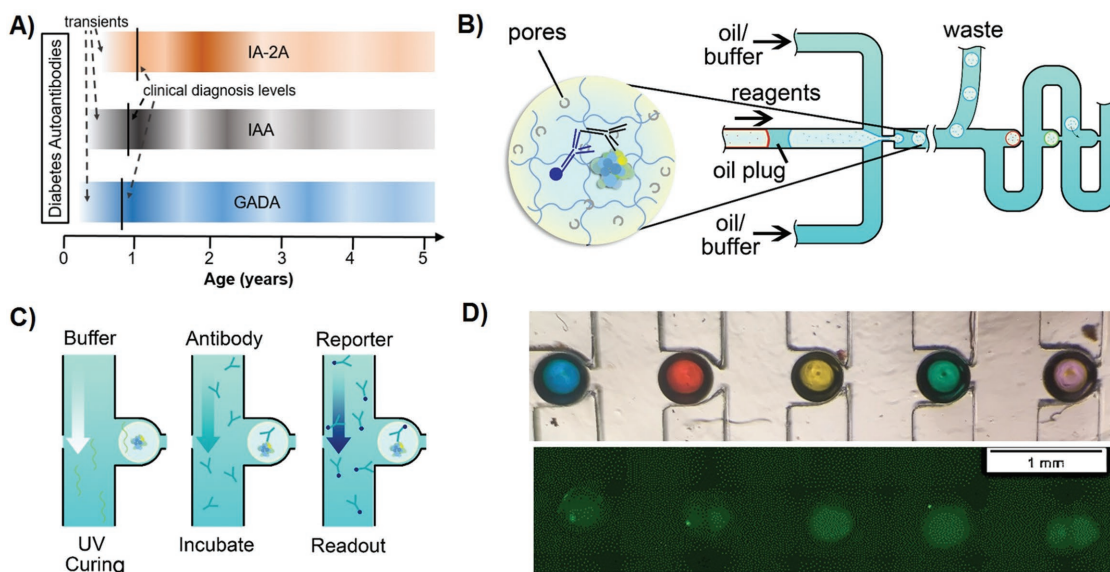
Figure 1. Quantitative microfluidic droplet array for diabetes detection panel. A) The rise and change of diabetes autoantibodies vary in individuals, and can be observed as early as 1 year of age, demonstrating the need for sensitive detection of multiple autoantibodies. B) We engineered a microfluidic array that generated individual porous droplets with detection chemistries optimized for the insulin, GAD, and IA-2 antibody detections. These "smart microgels" were then spatially arrayed in designated traps within the serpentine channels. This spatial multiplexing was achieved by flow switching of unwanted droplets to a waste channel, and redirecting droplets back toward the traps when the correct detection chemistry is generated. C) The serpentine microchannels allowed trapped droplets to be perfused by assay reagents. Buffer perfusion after UV curing allowed the porogen molecules (yellow stripes) to be washed away, creating a porous hydrogel droplet. Target antibodies (blue) and reporter antibodies (green) were then subsequently introduced into the microchannels, completing the immunoassay protocol. D) The result of spatial multiplexing was an array of droplets targeting individual diabetes antibodies, illustrated on top by the generation of multicolored droplets using food dyes. In the actual assay on bottom, only a single reporter wavelength was required, providing fluorescence intensities that varied at each spatial position per its respective antibody detection.

autoantibody detections below 10^{-11} mole L^{-1} (ng mL^{-1}) range, respectively. However, these separate improvements to autoantibody detections have not yet offered a combined sensitivity and multiplexing in a single volume assay.

We addressed these needs for the diabetes detection panel by creating an enhanced suspension assay multiplexed in microfluidic channels. Standard suspensions assays based on polystyrene beads, hydrogels, multicolored Luminex beads, Illumina's VeraCode particles, and novel plasmonic multiplexed substrates share advantages of flexible probe chemistry, inert surfaces, radial diffusion, smaller sample size, and lower costs.[15,42–47] Our group has further advanced the suspension assay technology by creating porous polyethylene glycol (PEG) hydrogel—"smart microgels"—to enhance the diffusion of biomolecules within the droplets, an improvement to the microscaled substrate that defines suspension assays.[48–50] In that previous work, we have demonstrated that the porosity generated by 20 kDa PEG optimized the diffusion of 250 kDa fluorescein isothiocyanate (FITC)-dextran into the hydrogel. This is larger than the 65 kDa antibodies used in this multiplexed assay, ensuring analyte access through the droplet volume. Furthermore, these microgels are arranged in a microfluidic serpentine array for multiplexing.[51] The microfluidic flow pushes the soluble reagents closer to the substrate surface, which is otherwise shielded by the boundary layers in bulk flows. These porosity and microfluidic advantages enhance the reagent transport and turnover throughout the whole droplet volume, enabling pg mL^{-1} protein detections with shortened assay time

of less than 2 h in previous works.[50,51] Here, we leveraged our smart microgels further for multiplexed detection of diabetes antibodies, aided by the microfluidic enhancement of analyte transport (Figure S1, Supporting Information). The multiplexed diabetes panel was optimized with recombinant proteins and antibodies to push the performance envelop of detections, toward serum measurements in the future. The result is a quantitative, faster, and single sample multiplexed detection panel for insulin, GAD, and IA-2 antibodies. Finally, the platform can be easily adapted for future antibodies such as zinc transporter 8.[52–54] Potential clinical applications of this detection panel may enable detailed immune profiling in T1D, and pave the way for a robust tool for early screening.
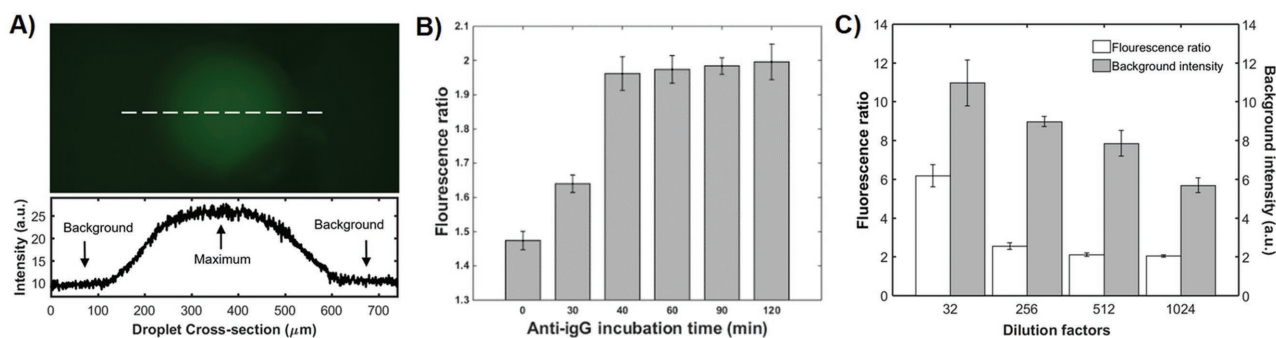
2. Results and Discussion

2.1. Sequential Arraying of Enhanced Droplets for Multiplexed Detection

Smart microgel optimizations were leveraged for the detection of diabetes antibodies by immobilizing capture antigens instead of capture antibodies. Detection chemistry, including diacrylated antigens in polyethylene diacrylate hydrogels and PEG porogen, was loaded into a microfluidic cross-junction (Figure 1B). Flow from this aqueous phase was then pinched by mineral oil at the junction, creating an instability that ejects 500 µm droplets at a predictable frequency.[50] Droplets then

ADVANCED
SCIENCE NEWS
www.advancedsciencenews.com

NANO · MICRO
small
www.small-journal.com

flowed down the serpentine channels and occupied individual trap sites one after another. However, in order to generate multiplexed detections for insulin, GAD, and IA-2 antibodies in a single channel, droplets with different capture molecules were generated and sequentially trapped. This was achieved by directing the unwanted droplets toward a waste channel, then switching the flow toward the serpentine traps once desired droplets were generated (Figure 1B). Upon trapping, the droplets were UV cured to immobilize the capture antigens and solidify the hydrogel for washing in TBST (Tris-buffered Saline and Tween 20) to remove porogens (Figure 1C). With porosity-enhanced mass transport, unreacted porogen was thoroughly removed after 4.5 h of microfluidic perfusion, compared to the 24 h of incubation needed for bulk preparations.[50] The resultant array (Figure 1D) represented a spatially multiplexed diabetes detection panel, without issues associated with spectral overlapping or computational imaging algorithms for shape-coded techniques. After formation of the multiplexed smart microgels, the array was then ready to be assayed by flowing target antibodies, reporter antibodies, and washing steps, optimized in the following section.

2.2. Optimization of Reporter Incubation Time and Dilution Factor

The detections of all three antibodies shared a common reporter, FITC-labeled IgG, whose incubation time and dilution factor were optimized using the insulin antibody detection. The fluorescence readout from the detection was quantified by the maximum droplet intensity divided by the background intensity, as illustrated by the line scan in **Figure 2**A. Using this quantification, reporter readout plateaued after 40 min of incubation (Figure 2B). Furthermore, the reporter dilution showed lowered background and useful signal up to 1024 X dilution, which dramatically reduced the usage of reporter reagents (Figure 2C). Based on these results, all subsequent experiments were carried out with 40 min of reporter incubation at 1024 X dilution. We anticipate the lower background from reporter dilution may help reduce nonspecific signals when moving to serum-based detections in the future.

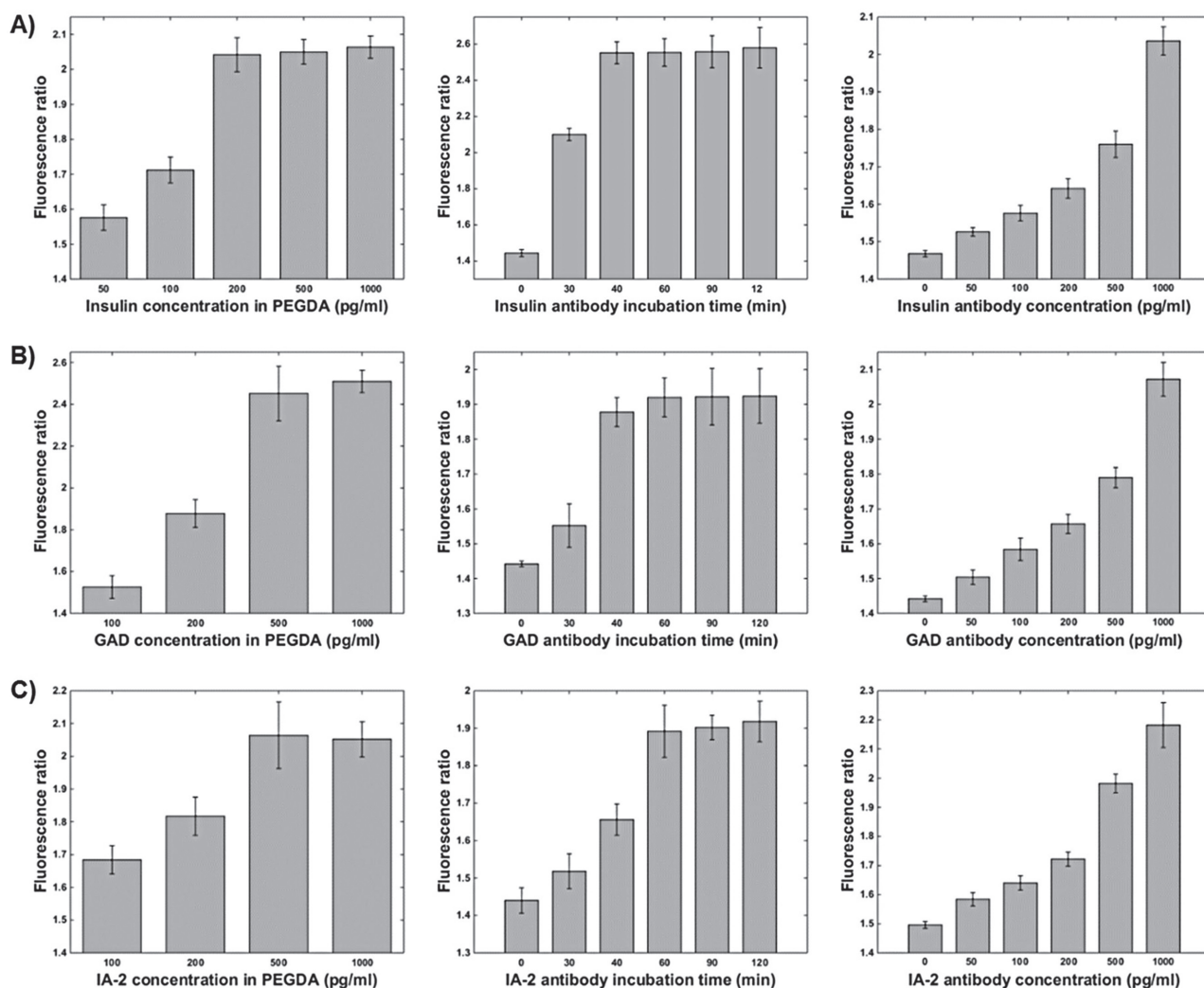## 2.3. Optimization of Capture Antigens Concentration in PEGDA

After reporter optimization, the capture antigen concentration corresponding to each target antibody was optimized. All antigen optimizations were incubated with 1000 pg mL^{-1} target antibodies. **Figure 3**A illustrates the insulin capture antigen optimization, where the fluorescence ratio plateaued above a concentration of 200 pg mL^{-1}. GAD antigen optimization is shown in Figure 3B, where the fluorescence ratio showed a plateau above 500 pg mL^{-1}. Similarly, Figure 3C shows that IA-2 concentration in poly(ethylene) glycol diacrylate (PEGDA) plateaus above 500 pg mL^{-1}. Optimization of antigen immobilization illustrated the differences of the binding epitopes between each antigen–antibody pair.[23–36] The subsequent experiments were run at their respective optimized antigen concentrations.

2.4. Optimization of Target Antibodies Incubation Time

Next, we considered the kinetics of antibody–antigen binding within the smart microgels by optimizing the target antibody incubation times. Smart microgels immobilized with aforementioned antigen concentrations were incubated for various durations with their respective antibodies. The fluorescence ratio for insulin detection improved up to 40 min of target antibody incubation and plateaued thereafter (Figure 3A). The same was seen for GAD antibody with a plateau after 40 min (Figure 3B). IA-2 and its antibody showed a different kinetics, as optimal incubation did not occur until after 60 min (Figure 3C). We should also note that IA-2 antibody is sensitive to buffer conditions, where glycine additives would increase nonspecific binding to the PEG hydrogel. Based on these optimizations, the longest incubation time was 60 min for the IA-2 antibody, which we adopted for all subsequent singleplexed and multiplexed detections.

2.5. Characterizing the Limits of Antibody Detections

The assay protocol described above was optimized at 1000 pg mL^{-1} for respective diabetes antibodies. We subsequently

Figure 2. Reporter optimization. A) All fluorescence measurements were quantified by the ratio of maximum center intensity normalized by the background intensity, as seen by the line scan across a typical droplet. B) Fluorescence ratio of the reporter plateaued after 40 min of reporter incubation. C) While fluorescence ratio flattened after 256 times reporter dilution, the noise continued to drop. We selected the reporter dilution of 1024 times to reduce reagent consumption and minimize the background intensity, which would provide smaller standard deviations for more sensitive detections.

ADVANCED
SCIENCE NEWS
www.advancedsciencenews.com

NANO MICRO
small
www.small-journal.com

Figure 3. Diabetes panel optimization. A) Insulin antibody detection was optimized with 200 pg mL⁻¹ capture antigen immobilization, 40 min of analyte incubation, and a detectivity curve with a detection limit of 19.6 pg mL⁻¹. B) GAD antibody detection was optimized with a 500 pg mL⁻¹ capture antigen immobilization, 40 min of analyte incubation, and a detectivity curve with a detection limit of 18.7 pg mL⁻¹. C) IA-2 antibody detection was optimized with a 500 pg mL⁻¹ capture antigen immoblization, 60 min of analyte incubation, and a detectivity curve with a detection limit of 12.7 pg mL⁻¹. All capture antigen and analyte incubation optimizations were completed in triplicates. All detectivity curves were completed with five replicate runs. Error bars denote standard deviations.

tested the detectivity below this concentration to characterize the detection limits for each antibody. Concentrations of 50, 100, 200, 500, and 1000 pg mL⁻¹ were assayed in five runs for each antibody, with error bars denoting standard deviations between each assay run at the particular concentration (Figure 3). The detection limit was defined to be the concentration at which the signal rises three times the standard deviations of the zeroth concentration. Using this definition, the insulin antibody detection limit was found to be 19.6 pg mL⁻¹ (Figure 3A). The GAD antibody detection limit was found to be 18.7 pg mL⁻¹ (Figure 3B). The IA-2 antibody detection limit was found to be 12.7 pg mL⁻¹ (Figure 3C). Since the detection limit is a function of the background fluorescence and slope of the detectivity curve, minimization of reporter antibody contributed to these enhanced detection limits (Figure 2C).

2.6. Characterization of Assay Specificity

To investigate whether other protein components in serum could potentially affect the fluorescence ratio, antigen immobilized microgel droplets were incubated with phosphate buffered saline (PBS), 0.1% bovine serum albumin (BSA), and their respective antibodies at 1000 pg mL⁻¹ (**Figure 4**). Antibody detections yielded fluorescence ratios higher than 2, whereas PBS and BSA yielded background levels of 1.5 or lower. More importantly, errors bars showed significant differences between specific and background detections with $p < 0.0001$. One reason for the low background without blocking is the bioinert nature of PEG hydrogel against nonspecific antibody binding. The result indicated that proteins other than targeted diabetes antibodies had minimum contributions toward the fluorescent

ADVANCED
SCIENCE NEWS
www.advancedsciencenews.com

NANO · MICRO
small
www.small-journal.com
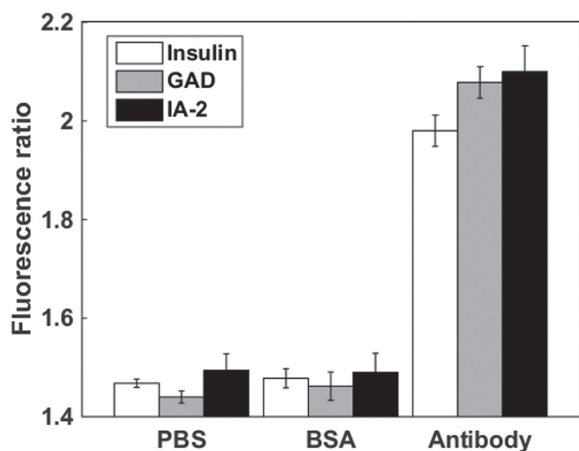
Figure 4. Assay specificity. Nonspecific binding to BSA resulted in fluorescence ratios on par with PBS background. Specific antibody detections resulted in a ratio around 2 versus 1.5 of background. Moreover, significant differences between detections and background yielded a $p < 0.0001$.

signal, and also demonstrated that antigen functionalization without additional blocking is sufficient for smart microgel specificity.

2.7. Characterization of Singleplex and Duplex Cross-Reactivity

One major difficulty in assaying multiple antibodies within one sample assay volume is the cross-reactivity among the target antibodies and nontarget proteins. First, microgel droplets of all target antigens were incubated with each target antibody one at a time at 1000 pg mL^{-1} to evaluate antigen–antibody cross-reactivity (**Figure 5**). For reference, background fluorescence ratios for each antigen (zero antibody concentrations) were typically below 1.5, as seen from their detectivity curves. In comparison, the on-target antigen–antibody detections, e.g., insulin to insulin antibody, yielded a ratio close to 2, significantly higher than the background ($p < 0.0001$, complete comparisons in Table S1, Supporting Information). After

analysis of singleplex cross-reactivity, combinations of two antibodies each at 1000 pg mL^{-1} were assayed (**Figure 6**). As singleplex cross-reactivity showed negligible nonspecific bindings between antibody and capture antigens, this duplex assay tested the possibility of unintended antibody to antibody interactions. Again, the on-target pairs yielded fluorescence ratios close to 2, while miss-matched backgrounds remained below 1.5. For example, the GAD to insulin+GAD antibodies fluorescence ratio was significantly higher than that of the IA-2 miss-matched with insulin+GAD antibodies ($p < 0.0001$, 2D plots and complete statistics in Figure S2 and Table S1, Supporting Information).

### 2.8. Muliplexed Detection and Quantitative Protein Recovery

After confirming negligible cross-reactivities at elevated antibody concentrations, we demonstrated multiplexed detections of insulin, GAD, and IA-2 antibody concentrations and their quantifications simultaneously. Three concentrations of 50, 200, and 500 pg mL^{-1} were assayed for each target antibody in multiplexed droplets. Triplicates were run for each condition. However, since the detections were multiplexed, the entire assay took a total of just nine runs. The measured concentrations were within 15% of the designated values (**Table 1**).

3. Discussion

The diabetes detection panel presented here achieved detection limits better than 20 pg mL^{-1} for all three target antibodies optimized. For reference, the recombinant antibodies used in this detection panel weighed less than 65 kDa, which means around just 8–30 thousand molecules were detected in each 500 µm droplet. This level of detection is orders of magnitude below serum levels of insulin, GAD, and IA-2 autoantibodies in nondiabetic patients, nominally at 2.4 ng mL^{-1}. However, that threshold for T1D diagnosis does not account for the low level transients before the rise of antibody levels in serum, which can
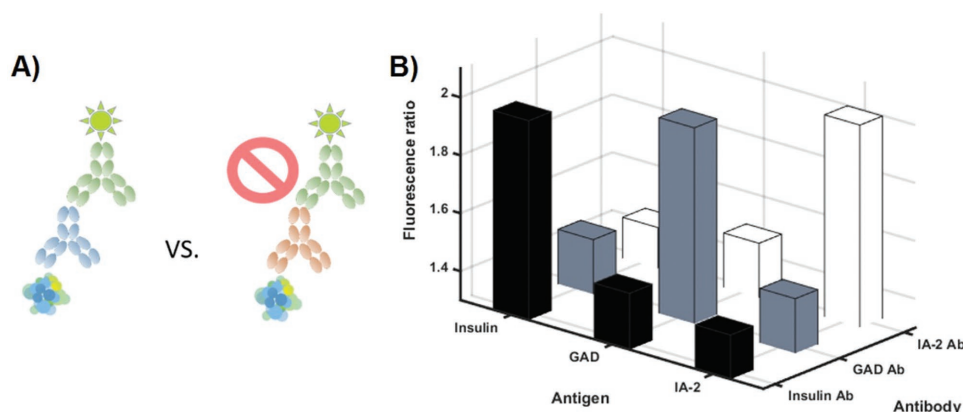
Figure 5. Singleplex cross-reactivity. A) Cross-reactivity between target (blue) and nontarget (orange) antibodies are tested one at a time to investigate nonspecific antibody–antigen interactions. B) This test showed that nonspecific antibody–antigen reactions yielded fluorescence ratios similar to that of background at ≈1.5.

ADVANCED
SCIENCE NEWS
www.advancedsciencenews.com

NANO · MICRO
small
www.small-journal.com
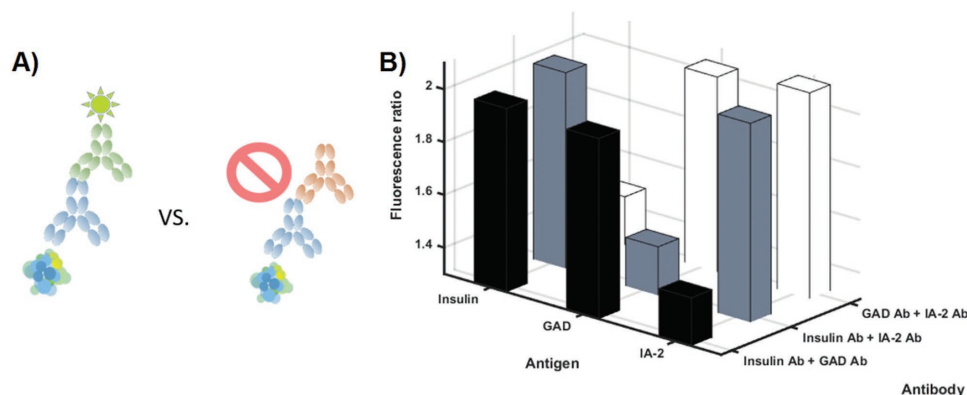
Figure 6. Duplex cross-reactivity. A) Cross-reactivity between combinations of antibodies pairs tested nonspecific antibody–antibody interactions. B) This test showed that nonspecific antibody–antibody reactions did not affect the on-target antibody–antigen detections.

be present in patients as young as 1 year of age.[22] With a sensitive, multiplexed detection panel, at-risk patients and siblings or family members of diabetics can receive early screening and frequent monitoring for the development of diabetes, before any hyperglycemia has manifested.

One major benefit of the smart microgel antibody detection is its inert hydrogel chemistry, which eliminates the need for blocking and reduces the assembly time for each assay. Next, the spatial multiplexing eliminates the possibility of spectral overlapping or complex shape coded imaging. Furthermore, the length for target incubation, reporter incubation, and two buffer washing times totaled 2 h—an accelerated protocol that is difficult to achieve by current antibody or RIA assays. Since the protein reagents are suspended in hydrogel substrates, their native conformation and binding kinetics can be preserved.[55–57] Moreover, enhanced hydrogel based substrates may demonstrate better storage capabilities,[58–60] enabling pregenerated, prepackaged diabetes detection panels for wider distribution and assay adaptation. Additionally, newly identified neoantigens[23–36] and ZnT8[52–54] can be rapidly added in a future multiplexed version of the diabetes panel, to enable clinical investigations of their predicative and screening values,[4–7] plus potential disease mechanisms. Lastly, available hydrogel functionalities can also enable immobilization of short peptides, nucleotides, aptamer, reverse transcription amplification, or cell encapsulates to create novel detection schemes or beta cell stimulations,[61–66] all of which can benefit from the enhanced hydrogel kinetics and multiplexing presented in this work. Coupled with the microfluidic serpentine's ability to manipulate soluble concentrations, the smart microgel platform provides a highly useful in vitro tool to study diabetes mechanisms.

4. Conclusion

We have achieved a multiplexed detection panel for diabetes antibodies targeting insulin, GAD, and IA-2. The assay can be prepared in 4.5 h prior to running the assay, with a total assay time of just 2 h for all three parameters in a single sample. For all target antibodies, a detection limit better than 20 pg mL^{-1} was achieved, representing the detection of only 8–30 thousand molecules in each microgel droplet. Singleplex and multiplex detections showed negligible cross-reactivity. Multiplexed detections were within 15% of the target concentrations. The serpentine microfluidic achieved a spatial multiplexing of the microgels that avoided issues associated with spectral or imaging based techniques. The resultant detection panel has the potential to improve diabetes detection, as well as investigate immunogenic mechanisms in diabetes.

5. Experimental Section

Reagents Preparations: Yeast host recombinant human insulin, recombinant protein GAD 2, anti-GAD$_{65}$ (mouse anti-human), and recombinant IA-2 proteins were procured from Sigma-Aldrich. Mouse anti-human anti-insulin, anti-IA2 antibodies (mouse anti-human), and goat anti-mouse FITC labeled IgG were procured from Millipore. PEGDA ($M_n \approx 6000$), PEG ($M_n \approx 20,000$), photoinitiator (2-hydroxy-4'-(2-hydroxyethoxy)-2 methylpropiophenone), PBS, and BSA were procured from Sigma-Aldrich. Acrylate poly (ethylene) glycol succinimidyl carboxymethyl, *Mn* 5000, (ACRL-PEG-SCM-5000) was obtained from Laysan Bio Inc. (Arab, AL).

To immobilize the antigens within the microgel, the antigens were incubated with 1.25 mg of ACRL-PEG-SCM-5000 in PBS at room temperature for 3 h prior to use and discarded afterward. The prepolymer solution consisting of 100 µL of 8% (w/v) of PEG6000DA, 2% (w/v) photoinitiator, 10% (w/v) PEG 20K, and acrylated antigen was then loaded in the microfluidics for droplet generation.

Droplet Generation: The prepolymer solution was introduced at 1 µL min^{-1}, and mineral oil was introduced at 15 µL min^{-1} to generate the droplets at the microfluidic cross-junction. When one of the generated droplets was flown in to the serpentine pockets, its trapping blocked the cross-serpentine flow and redirected the next droplet toward the following pocket sequentially. After trapping, droplets were exposed to ultraviolet light for crosslinking for 5 min (UVP CL-1000 UV Oven, 365 nm). Then, BSA buffer was flown in at 30 µL min^{-1} to continuously wash the droplet for 30 min to prevent polydimethylsiloxane (PDMS) protein absorption. Lastly, PBS was flown in at 30 µL min^{-1} to

Table 1. Multiplexed protein detections with target concentrations of 50, 200, and 500 pg mL^{-1} for all three antibodies simultaneously.

Target concentration [pg mL^{-1}]			Retrieved concentration [pg mL^{-1}]		
Insulin Ab	GAD Ab	IA-2 Ab	Insulin Ab	GAD Ab	IA-2 Ab
50	50	50	48 ± 11.4	45 ± 7.1	51.8 ± 9.8
200	200	200	204 ± 22.8	201.4 ± 17.8	203.3 ± 26.3
500	500	500	494.9 ± 41.7	521.28 ± 26.24	520 ± 39.5

continuously wash the droplets for 4 h to remove the unreacted reagents and PEG porogens, thus creating the porous microgel.

Assay Protocol: For multiplexed detection, different prepolymers containing different acrylated antigens were loaded in the microfluidic tubing (Tygon tubing 1/16 in. ID) separated by mineral oil plugs. The prepolymers were then delivered into the microfluidics using a syringe pump to generate droplets. After generating and trapping droplets with the first prepolymer reagent, subsequent unwanted droplets were redirected to the waste channel. Then, the waste channel was closed to allow droplets with the second prepolymer containing the next acrylated antigen to be flown in and trapped in the next serpentine trap. The process continued until all three prepolymers containing the three different capture antigens were trapped in designated spots. These smart microgel droplets were then UV-cured and washed as described above.

To run the multiplexed assays, smart microgels were incubated with appropriate antibodies at 20 µL min^{-1} flow rate for 60 min. Then, they were washed with TBST at 30 µL min^{-1} for 15 min and subsequently incubated with the reporter antibody at 30 µL min^{-1} for 40 min. Following this, droplets were washed again with TBST for 5 min and then imaged under the fluorescence microscopy.

Fluorescence Data and Statistical Analysis: After all the reactions between antigens, antibodies, and reporter antibody were completed, the smart microgel droplets were imaged under fluorescence microscopy for readout. The ratio of maximum center droplet intensity over background intensity was calculated using ImageJ to provide a normalized intensity value. The noise of the data is then the standard deviations of the normalized values. All optimization and cross-reactivity were done in triplicates, while the detection curve was done with five repeated runs. To generate the statistics, detections were compared to background by individual-samples *t*-test. The *p*-values (double sided) were provided for interpretation (Table S1, Supporting Information).

Supporting Information

Supporting Information is available from the Wiley Online Library or from the author.

Acknowledgements

Conflict of Interest

The authors declare no conflict of interest.

Keywords

[1] C. Törn, P. W. Mueller, M. Schlosser, E. Bonifacio, P. J. Bingley, *Diabetologia* **2008**, *51*, 846.

[2] T. P. Staeva, L. Chatenoud, R. Insel, M. A. Atkinson, *Diabetes* **2013**, *62*, 9.

[3] J. M. Wenzlau, J. C. Hutton, *Curr. Diabetes Rep.* **2013**, *13*, 608.

[4] C. J. Greenbaum, J. P. Palmer, B. Kuglin, H. Kolb, *J. Clin. Endocrinol. Metab.* **1992**, *74*, 1040.

[5] M. Schlosser, P. W. Mueller, C. Törn, E. Bonifacio, P. J. Bingley, *Diabetologia* **2010**, *53*, 2611.

[6] V. Lampasona, M. Schlosser, P. W. Mueller, A. J. Williams, J. M. Wenzlau, J. C. Hutton, P. Achenbach, *Clin. Chem.* **2011**, *57*, 1693.

[7] P. J. Bingley, E. Bonifacio, P. W. Mueller, *Diabetes* **2003**, *52*, 1128.

[8] M. A. Atkinson, N. K. Maclaren, W. J. Riley, W. E. Winter, D. D. Fisk, R. P. Spillar, *Diabetes* **1986**, *35*, 894.

[9] A. J. Williams, V. Lampasona, M. Schlosser, P. W. Mueller, D. L. Pittman, W. E. Winter, B. Akolkar, R. Wyatt, C. Brigatti, S. Krause, P. Achenbach, *Diabetes* **2015**, *64*, 3239.

[10] C. Andersson, M. Kolmodin, S. A. Ivarsson, A. Carlsson, G. Forsander, B. Lindblad, J. Ludvigsson, I. Kockum, C. Marcus, U. Samuelsson, E. Örtqvist, *Pediatr. Diabetes* **2014**, *15*, 336.

[11] J. M. LaGasse, M. S. Brantley, N. J. Leech, R. E. Rowe, S. Monks, J. P. Palmer, G. T. Nepom, D. K. McCulloch, W. A. Hagopian, *Diabetes Care* **2002**, *25*, 505.

[12] C. F. Verge, R. Gianani, E. Kawasaki, L. Yu, M. Pietropaolo, H. P. Chase, G. S. Eisenbarth, R. A. Jackson, *Diabetes* **1996**, *45*, 926.

[13] A. G. Ziegler, S. Schmid, D. Huber, M. Hummel, E. Bonifacio, *JAMA* **2003**, *290*, 1721.

[14] Z. Zhao, D. Miao, A. Michels, A. Steck, F. Dong, M. Rewers, L. Yu, *J. Immunol. Methods* **2016**, *430*, 28.

[15] B. Zhang, R. B. Kumar, H. Dai, B. J. Feldman, *Nat. Med.* **2014**, *20*, 948.

[16] L. Herszenyi, Z. Tulassay, *Dig. Dis.* **2012**, *30*, 201.

[17] L. Yu, D. T. Robles, N. Abiru, P. Kaur, M. Rewers, K. Kelemen, G. S. Eisenbarth, *Proc. Natl. Acad. Sci. USA* **2000**, *97*, 1701.

[18] P. J. Bingley, E. Bonifacio, A. G. Ziegler, D. A. Schatz, M. A. Atkinson, G. S. Eisenbarth, *Diabetes Care* **2001**, *24*, 398.

[19] A. D. Liese, R. B. D'Agostino Jr, R. F. Hamman, P. D. Kilgo, J. M. Lawrence, L. L. Liu, B. Loots, B. Linder, S. Marcovina, B. Rodriguez, D. Standford, D. E. Williams, **2006**, *118*, 1510.

[20] C. C. Patterson, G. G. Dahlquist, E. Gyürüs, A. Green, G. Soltész, *Lancet* **2009**, *373*, 2027.

[21] K. G. M. M. Alberti, P. Z. Zimmet, *Diabetic Med.* **1998**, *15*, 539.

[22] E. Bonifacio, *Diabetes Care* **2015**, *38*, 989.

[23] M. J. Kracht, A. Zaldumbide, B. O. Roep, *Trends Endocrinol. Metab.* **2016**, *27*, 353.

[24] S. M. Trigwell, P. M. Radford, S. R. Page, A. C. Loweth, R. F. James, N. G. Morgan, I. Todd, *Clin. Exp. Immunol.* **2001**, *126*, 242.

[25] M. van Lummel, G. Duinkerken, P. A. van Veelen, A. de Ru, R. Cordfunke, A. Zaldumbide, I. Gomez-Touriño, S. Arif, M. Peakman, J. W. Drijfhout, B. O. Roep, *Diabetes* **2014**, *63*, 237.

[26] J. W. McGinty, I. T. Chow, C. Greenbaum, J. Odegard, W. W. Kwok, E. A. James, *Diabetes* **2014**, *63*, 3033.

[27] I. Kharroubi, L. Ladrière, A. K. Cardozo, Z. Dogusan, M. Cnop, D. L. Eizirik, *Endocrinology* **2004**, *145*, 5087.

[28] D. R. Laybutt, A. M. Preston, M. C. Åkerfeldt, J. G. Kench, A. K. Busch, A. V. Biankin, T. J. Biden, *Diabetologia* **2007**, *50*, 752.

[29] S. C. Martinez, K. Tanabe, C. Cras-Méneur, N. A. Abumrad, E. Bernal-Mizrachi, M. A. Permutt, *Diabetes* **2008**, *57*, 846–59.

[30] K. Maedler, G. A. Spinas, D. Dyntar, W. Moritz, N. Kaiser, M. Y. Donath, *Diabetes* **2001**, *50*, 69.

[31] D. A. Cunha, P. Hekerman, L. Ladrière, A. Bazarra-Castro, F. Ortis, M. C. Wakeham, F. Moore, J. Rasschaert, A. K. Cardozo, E. Bellomo, L. Overbergh, *J. Cell Sci.* **2008**, *121*, 2308.

[32] B. O. Roep, M. J. Kracht, M. van Lummel, A. Zaldumbide, *Curr. Opin. Immunol.* **2016**, *43*, 67.

[33] M. S. Horwitz, L. M. Bradley, J. Harbertson, T. Krahl, J. Lee, N. Sarvennick, *Nat. Med.* **1998**, *4*, 781.

[34] B. T. Kurien, R. H. Scofield, *Autoimmun. Rev.* **2008**, *7*, 567.

ADVANCED
SCIENCE NEWS
www.advancedsciencenews.com

NANO MICRO
small
www.small-journal.com

[35] D. L. Kaufman, M. Clare-Salzler, J. Tian, T. Forsthuber, G. S. Ting, P. Robinson, M. A. Atkinson, E. E. Sercarz, A. J. Tobin, P. V. Lehmann, *Nature* **1993**, *366*, 69.

[36] S. Hong, M. T. Wilson, I. Serizawa, L. Wu, N. Singh, O. V. Naidenko, T. Miura, T. Haba, D. C. Scherer, J. Wei, M. Kronenberg, *Nat. Med.* **2001**, *7*, 1052.

[37] L. Yu, D. Miao, L. Scrimgeour, K. Johnson, M. Rewers, G. S. Eisenbarth, *Diabetes* **2012**, *61*, 179.

[38] R. Hilbrands, V. A. Huurman, P. Gillard, J. H. L. Velthuis, M. De Waele, C. Mathieu, L. Kaufman, M. Pipeleers-Marichal, Z. Ling, B. Movahedi, D. Jacobs-Tulleneers-Thevissen, D. Monbaliu, D. Ysebaert, F. K. Gorus, B. O. Roep, D. G. Pipeleers, B. Keymeulen, *Diabetes* **2009**, *58*, 2267.

[39] Mayo Medical Laboratories, *Mayo Medical Laboratories Interpretive Handbook*, Mayo Medical Laboratories, Rochester, NY, USA **2005**.

[40] D. Miao, K. M. Guyer, F. Dong, L. Jiang, A. K. Steck, M. Rewers, G. S. Eisenbarth, L. Yu, *Diabetes* **2013**, *62*, 4174.

[41] L. Yu, F. Dong, D. Miao, A. R. Fouts, J. M. Wenzlau, A. K. Steck, *Diabetes Care* **2013**, *36*, 2266.

[42] M. Evans, C. Sewter, E. Hill, *Assay Drug Dev. Technol.* **2003**, *1*, 199.

[43] J. P. Nolan, L. A. Sklar, *Trends Biotechol.* **2002**, *20*, 9.

[44] S. C. Chapin, D. C. Pregibon, P. S. Doyle, *Lab Chip* **2009**, *9*, 3100.

[45] L. Wang, C. Yang, W. Tan, *Nano Lett.* **2005**, *5*, 37.

[46] B. He, S. J. Son, *Anal. Chem.* **2007**, *79*, 5257.

[47] S. Birtwell, *Integr. Biol.* **2009**, *1*, 345.

[48] A. A. Al-Ameen, G. Ghosh, *Biosens. Bioelectron.* **2013**, *49*, 105.

[49] M. A. Al-Ameen, J. Li, D. G. Beer, G. Ghosh, *Analyst* **2015**, *140*, 4530.

[50] Z. Zhao, M. A. Al-Ameen, K. Duan, G. Ghosh, J. F. Lo, *Biosens. Bioelectron.* **2015**, *74*, 305.

[51] K. Duan, G. Ghosh, J. F. Lo, in *MicroTAS* (Eds. N. Pamme, J. Ducree) The Chemical and Biological Microsystems Society, Washington, DC, USA **2016** p. 956.

[52] G. Huang, Y. Xiang, L. Pan, X. Li, S. Luo, Z. Zhou, *Diabetes/Metab. Res. Rev.* **2013**, *29*, 363.

[53] F. K. Gorus, E. V. Balti, I. Vermeulen, S. Demeester, A. Van Dalem, O. Costa, H. Dorchy, S. Tenoutasse, T. Mouraux, C. De Block, P. Gillard, *Clin. Exp. Immunol.* **2013**, *171*, 82.

[54] M. Fabris, S. Zago, M. Liguori, M. T. Trevisan, M. Zanatta, A. Comici, G. Zanette, E. Carlin, F. Curcio, E. Tonutti, *Autoimmun. Highlights* **2015**, *6*, 17.

[55] J. Kopeček, *Biomaterials* **2007**, *28*, 5185.

[56] E. Cosgriff-Hernandez, M. S. Hahn, B. Russell, T. Wilems, D. Munoz-Pinto, M. B. Browning, J. Rivera, M. Höök, *Acta Biomater.* **2010**, *6*, 3969.

[57] M. C. Branco, D. J. Pochan, N. J. Wagner, J. P. Schneider, *Biomaterials* **2010**, *31*, 9527.

[58] S. Frokjaer, D. E. Otzen, *Nat. Rev. Drug Discovery* **2005**, *4*, 298.

[59] M. Ye, S. Kim, K. Park, *J. Controlled Release* **2010**, *146*, 241.

[60] R. E. Sallach, W. Cui, F. Balderrama, A. W. Martinez, J. Wen, C. A. Haller, J. V. Taylor, E. R. Wright, R. C. Long, E. L. Chaikof, *Biomaterials* **2010**, *31*, 779.

[61] L. Li, Q. Wang, J. Feng, L. Tong, B. Tang, *Anal. Chem.* **2014**, *86*, 5101.

[62] H. Zhang, G. Jenkins, Y. Zou, Z. Zhu, C. J. Yang, *Anal. Chem.* **2012**, *84*, 3599.

[63] E. Brouzes, M. Medkova, N. Savenelli, D. Marran, M. Twardowski, J. B. Hutchison, J. M. Rothberg, D. R. Link, N. Perrimon, M. L. Samuels, *Proc. Natl. Acad. Sci.* **2009**, *106*, 14195.

[64] A. Huebner, M. Srisa-Art, D. Holt, C. Abell, F. Hollfelder, J. B. Edel, *Chem. Commun.* **2007**, *12*, 1218.

[65] D. Chen, W. Du, Y. Liu, W. Liu, A. Kuznetsov, F. E. Mendez, L. H. Philipson, R. F. Ismagilov, *Proc. Natl. Acad. Sci.* **2008**, *105*, 16843.

[66] C. J. Easley, J. V. Rocheleau, W. S. Head, D. W. Piston, *Anal. Chem.* **2009**, *81*, 9086.